# Fréchet distribution in geometric graphs for drone networks

Maria Raftopoulou [1,*] Remco Litjens [1,2] and Piet Van Mieghem [1]

[1] *Faculty of Electrical Engineering, Mathematics and Computer Science, Delft University of Technology, P.O. Box 5031, 2600 GA Delft, The Netherlands*

[2] *Department of Networks, TNO, P.O. Box 96800, 2509 JE The Hague, The Netherlands*

(Received 13 April 2022; accepted 27 June 2022; published 9 August 2022)

In this paper, we focus on the link density in random geometric graphs (RGGs) with a distance-based connection function. After deriving the link density in $D$ dimensions, we focus on the two-dimensional (2D) and three-dimensional (3D) space and show that the link density is accurately approximated by the Fréchet distribution, for any rectangular space. We derive expressions, in terms of the link density, for the minimum number of nodes needed in the 2D and 3D spaces to ensure network connectivity. These results provide first-order estimates for, e.g., a swarm of drones to provide coverage in a disaster or crowded area.

DOI: 10.1103/PhysRevE.106.024301

## I. INTRODUCTION

Random graphs are created from a set of $N$ nodes, placed in a space $V \in \mathbb{R}^D$, where each pair of nodes is connected by a link with probability $p$, independently of the existence of any other link [1]. If the node $i$ at position $r_i$ and the node $j$ at position $r_j$ are connected with probability $p_{ij} = f(|r_i - r_j|)$, where $f(r)$ is a real function of the distance $r$, then we talk about a *random geometric graph* (RGG). If $f(r) = 1_{r<r_0}$, where $1_x$ is the indicator function,[1] then all nodes at distance smaller than $r_0$ are connected almost surely [2,3]. Moreover, the position $r_i$ of each node $i$ itself can be either deterministic or stochastic. In the latter case, the link existence is doubly stochastic and depends both on the distance function $f(r)$ and on the random placement of nodes described by a probability distribution $\Pr[r_1 \leqslant x_1, \cdots, r_N \leqslant x_N]$.

There is extensive work in literature on the properties of RGGs and their applications. RGGs can model transportation networks such as wireless [4,5] and airline [6] networks as well as infrastructural networks like power grids [7]. Also, RGGs can be applied in analyzing the structure of large data sets [8] and in modeling ad hoc networks, which are decentralized networks that do not rely on a fixed infrastructure. Applications of ad hoc networks include vehicular, disaster relief, sensor, and flying swarm robotics networks [9,10].

In this work, we focus on the *link density* and the *connectivity* of two-dimensional (2D) and three-dimensional (3D) RGGs, with an application to wireless networks. We define the link density as the ratio of the expected number of links over the maximum possible number of links in an undirected graph and the connectivity as the probability that a path exists between any pair of nodes in the graph. Bettstetter [5] studies the number of nodes needed to provide connectivity in a 2D RGGs and Dall and Christensen [11] provide the critical connectivity threshold in $D$ dimensions. Van Mieghem [12] presents the exact solution for the link density and the average number of paths between any two nodes, when the graph is randomly generated in a square. Erba *et al.* [8] compare the average number of subgraphs in highly dimensional RGGs characterized by indicator-based and exponential distance functions. Moreover, multiple approximations to the nodal degree in bounded spaces are performed [13–15], however they are related to the 2D space and to indicator-based distance functions.

Focusing on connectivity in wireless communications, Hekmat and Van Mieghem [16] derive the giant component size for 2D RGGs with a log-normal distance function and show that it is a good measure for connectivity. Ng *et al.* [17] provide upper and lower bounds for the critical density of 2D and 3D RGGs with a log-normal distance function and under the unit disk model. By distributing the nodes inside or on the surface of a sphere, Khalid and Durrani [18] provide exact expressions for the mean node degree and the node isolation probability. They leave as an open problem the derivation of these expressions when the nodes are distributed in a cube. Finally, Dettmann and Georgiou [19] derive the full connection probability in 2D and 3D convex domains for various distance functions.

The main contributions of this work are the following:

(1) We derive an exact expression for the link density for an RGG in a $D$-dimensional prism and any distance function $f(r)$ allowing its graph properties to be elegantly and accurately deduced from an Erdős-Rényi random graph $G_p(N)$, whose theory is well developed [1].

For 2D and 3D RGGs modeling wireless networks that are characterized by a simple distance-based path loss model and Rayleigh fading:

(2) We derive an approximation of the link density in a hypercube that illustrates the importance of the nodes placed in its corners.

*m.raftopoulou@tudelft.nl

[1] $1_x = 1$ if condition $x$ is true, else $1_x = 0$.

 

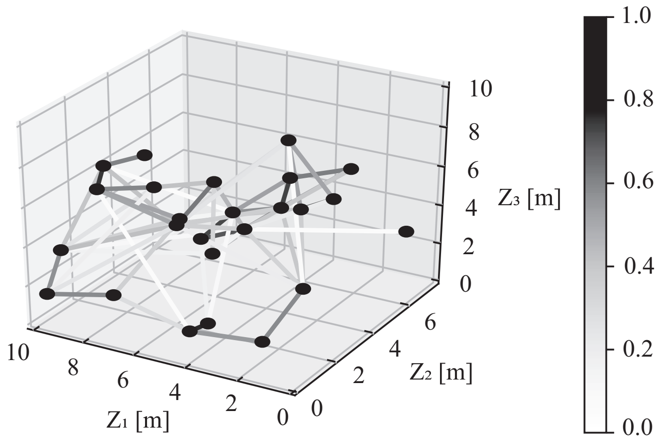


FIG. 1. Example realization of a RGG with $f(r) = e^{-0.07r^2}$ and $N = 25$ in a 3D rectangular prism, where the link color refers to the connection probability between two nodes. For visualization purposes, only links with $f(r) > 10^{-3}$ are shown.

(3) We analytically demonstrate how the link density depends on the path loss exponent and on the prism size and shape. We further show that the link density in the 3D space is smaller than or equal to that in the 2D space.

(4) We show that the complementary distribution function of the Fréchet distribution accurately approximates the link density for any path loss exponent, prism size, and prism shape.

(5) We deduce a general closed-form expression in terms of the link density to approximate the minimum density of nodes to ensure a connected network.

The paper is structured as follows. Section II describes the network model. The link density in the $D$-dimensional space is derived in Sec. III, which also presents an approximation of the link density in a hypercube. The impact of the wireless environment and the hyperprism's shape and volume on the link density is assessed in Sec. IV. Additionally, Sec. IV illustrates the high accuracy of the link density approximation with the Fréchet distribution as well as a brief motivation on the approximation accuracy. In Sec. V, we derive the minimum number of nodes needed for connectivity based on the link density. Finally, Sec. VI concludes the paper with a summary and the future work.

## II. NETWORK MODEL

A graph $G(N, L)$ consists of a set $\mathcal{N}$ of $N$ nodes and a set $\mathcal{L}$ of $L$ links. We assume that nodes are placed uniformly at random inside a hyperprism in $D$ dimensions, with one vertex at the origin and with length $Z_d$ in the $d$th orthogonal direction of the coordinate axes. The distance function $f(r)$ provides the connection probability between two nodes placed at $r_i = (r_{i_1}, \cdots, r_{i_D})$ and $r_j = (r_{j_1}, \cdots, r_{j_D})$, where $r = |r_i - r_j|$ denotes their mutual distance. Figure 1 draws an example of the considered graph with $f(r) = e^{-0.07r^2}$ in the 3D space.

In wireless networks, the distance function $f(r)$ is influenced by the wireless channel between the nodes. The RGG assumption on independent link existence for distinct node pairs, is approximate for wireless networks, because wireless transmissions interfere with each other, thus creating dependency between the node pairs. Wireless networks that operate on a dedicated frequency band or in isolation from other wireless networks and ensure orthogonal transmissions in, e.g., frequency or time, can be exactly modeled by RGGs.

The impact of the wireless channel is reflected by the received signal power $P_{rx,ij}$, which depends on the distance $r$ between the transmitter $i$ at location $r_i$ and the receiver $j$ at location $r_j$. The average signal attenuation over distance is given by the *path loss*, approximately characterized by a power law. Assuming antenna gains $G_i$ and $G_j$ at the transmitter and receiver, respectively, the received signal power $P_{rx,ij}$ is [20]

$$P_{rx,ij}(r) = P_{tx,ij} G_i G_j K \left(\frac{r_c}{r}\right)^{\gamma}, \tag{1}$$

with

$$K = \left(\frac{\lambda}{4\pi r_c}\right)^2 < 1,$$

where $P_{tx,ij}$ is the transmit power for communication from $i$ to $j$ in watts [W], $\lambda$ is the wavelength in meters [m], $r_c$ is the reference distance for the antenna far field in meters [m], $\gamma$ is the path loss exponent and $r > r_c$ is given in meters [m]. The reference distance $r_c \in [1, 100]$ depends on the propagation environment and on the antenna characteristics [20] while it further holds that $r_c \gg \lambda$, which implies $K < 1$. The range of the path loss exponent $\gamma$ also depends on the propagation environment with typical values [20] ranging between 2 and 6.5. Generally, the value of $\gamma$ is determined by empirical measurements. The smallest value $\gamma = 2$ corresponds to the ideal case of free-space propagation.

Ignoring interference and thus assuming independent links, the signal-to-noise ratio (SNR) $\Gamma_{ij}$ that the receiver $j$ experiences from the transmitter $i$ is given by

$$\Gamma_{ij}(r) = \frac{P_{rx,ij}(r)}{P_{\text{noise}}} = \frac{P_{tx,ij} G_i G_j K}{P_{\text{noise}}} \left(\frac{r_c}{r}\right)^{\gamma}, \tag{2}$$

where $P_{\text{noise}}$ is the thermal noise power. Assuming a fixed transmission power $P_{tx,ij} = P_{tx,ji} = P_{tx}$ at every node, two nodes $i$ and $j$ are connected if and only if the $\Gamma_{ij} = \Gamma_{ji}$ is greater than the SNR threshold $\Gamma_{\min}$. Therefore,

$$f(r) = \Pr[\Gamma_{ij}(r) > \Gamma_{\min}].$$

Using Eq. (2), this can be rewritten as $f(r) = \Pr[r < r_0]$, where

$$r_0 = r_c \left(\frac{P_{tx} G_i G_j K}{P_{\text{noise}}\, \Gamma_{\min}}\right)^{1/\gamma}, \tag{3}$$

and thus $r_0 \geqslant r_c$, denotes the *maximum allowed distance* between node $i$ and node $j$ such that they are connected.

Since the received power $P_{rx,ij}$ reduces with distance $r$, node $i$ has a spherical coverage area and thus any node $j$ located within a sphere with radius $r_0$ is connected to the node $i$. Hence, the distance function can be written as a step function $f(r) = 1_{r<r_0}$.

In reality, the received signal power $P_{rx,ij}$ varies randomly due to signal reflections, caused by the various objects in the environment. Specifically, the received signal consists of multiple copies of the transmitted signal, called *multipath*

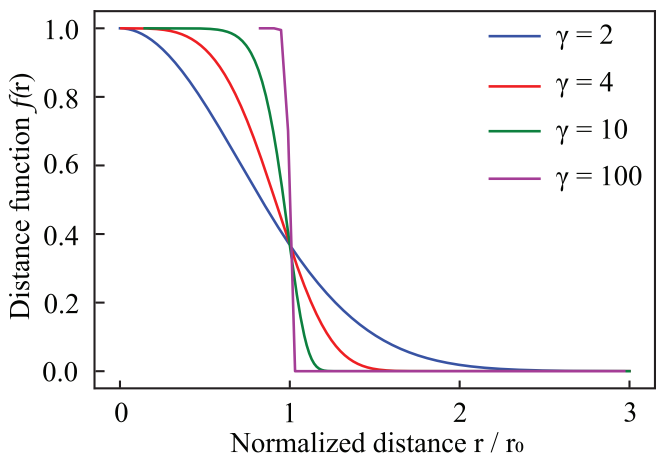


FIG. 2. Distance function $f(r)$ with respect to the normalized distance $\frac{r}{r_0}$ when $\beta = -127$ dB, $\lambda = 0.08$ m, and $r_c = 1$ m.

*fading*, where each copy is received with different power, at a different time and with a shift in phase and/or frequency. The movement of any object in the environment, including the transmitter and the receiver, may therefore lead to a received signal power variation, modeled by the time-varying nature of multipath fading. The received signal power $P_{rx,ij}$, at time $t$ and frequency $\nu$, is given by

$$P_{rx,ij}(r,t,\nu) = P_{tx}G_iG_jK\left(\frac{r_c}{r}\right)^{\gamma}||H_{i-j}(t,\nu)||^2, \tag{4}$$

where $H_{i-j}(t,\nu)$ is the channel response to multipath fading at time $t$ and frequency $\nu$ on the channel between transmitter $i$ and receiver $j$. With Eq. (4), the distance function $f(r) = \Pr[\Gamma_{ij}(r,t,\nu) > \Gamma_{\min}]$ can now be written as

$$f(r) = \Pr\left[||H_{i-j}(t,\nu)||^2 > \frac{\beta}{K}\left(\frac{r}{r_c}\right)^{\gamma}\right], \tag{5}$$

where $\beta$ is the *minimum required channel gain* given by

$$\beta = \frac{P_{\text{noise}}\,\Gamma_{\min}}{P_{tx}G_iG_j}. \tag{6}$$

Because generally $P_{\text{noise}} \ll P_{tx}$, we have $\beta < 1$. For a "typical" drone-to-drone application, it is estimated that $\beta < 10^{-10} = -100\ dB$.

Assuming that $H_{i-j}(t,\nu)$ is Rayleigh distributed [8], then $||H_{i-j}(t,\nu)||^2$ is exponentially distributed with a mean of 1 and Eq. (5) becomes

$$f(r) = e^{-\frac{\beta}{K}\left(\frac{r}{r_c}\right)^{\gamma}}. \tag{7}$$

The distance function in Eq. (7) is commonly considered in the literature with $r_c = 1\ m$ for wireless networks [19], while it also appears in studies on the properties of data sets and of machine learning algorithms [8] in highly dimensional RGGs. It is convenient to rewrite Eq. (7) with respect to the maximum allowed distance $r_0$, as derived for the case without multipath fading, using Eqs. (3) and (6):

$$f(r) = e^{-\left(\frac{r}{r_0}\right)^{\gamma}}, \tag{8}$$

for which $\lim_{\gamma\to\infty} f(r) = 1_{r<r_0}$ and $f(r_0) = \frac{1}{e} \approx 0.3678$.

Figure 2 illustrates the distance function $f(r)$ for different values of $\gamma$ in terms of the normalized distance, defined as the ratio of the distance $r$ over the maximum allowed distance $r_0$. A wider value range of $\gamma$ than [2,6.5] is considered to understand the behavior of the distance function $f(r)$ for all real, positive numbers. Figure 2 exemplifies that for a given $\gamma$, the distance function $f(r)$ reduces with distance $r$. Furthermore, the distance function $f(r)$ increases in $\gamma$ for $r < r_0$ but decreases in $\gamma$ for $r > r_0$ since with a higher $\gamma$, the received signal power $P_{rx,ij}$ attenuates more quickly over distance $r$.

## III. LINK DENSITY IN *D* DIMENSIONS

We define the link density $p = \frac{E[L]}{L_{\max}}$ as the ratio of the expected number $E[L]$ of links over the maximum possible number $L_{\max} = \frac{N(N-1)}{2}$ of links in an undirected graph. In this section, we derive the link density of a RGG in a rectangular hyperprism in $D$ dimensions and provide an approximation to the link density in a hypercube.

### A. Link density analysis

The number of links $L[\{\mathcal{R}\}]$ in a RGG with nodal positions $\{\mathcal{R}\} = \{r_1, r_2, \cdots r_N\}$ in space $V \in \mathbb{R}^D$ is given by [12]

$$L[\{\mathcal{R}\}] = \sum_{i=1}^{N}\sum_{j=i+1}^{N} f(|r_i - r_j|),$$

where $f(\cdot)$ is the function generating an RGG with $N$. The expected number of links $E[L]$ is given by

$$E[L] = \int_V \Pr[\{\mathcal{R}\}]L[\{\mathcal{R}\}]d[\{\mathcal{R}\}],$$

where $\Pr[\{\mathcal{R}\}] = g_{\{r_1,\cdots,r_N\}}(x_1,\cdots,x_N)$ is the probability density function (pdf) of the position of the set of nodes, given by

$$\Pr[\{\mathcal{R}\}] = \frac{d\Pr[r_1 \leqslant x_1,\cdots,r_N \leqslant x_N]}{dx_1\cdots dx_N},$$

resulting in

$$E[L] = \int_V dr_1\cdots dr_N\, g_{\{r_1,\cdots,r_N\}}(r_1,\cdots,r_N) \times \sum_{i=1}^{N}\sum_{j=i+1}^{N} f(|r_i - r_j|). \tag{9}$$

We can proceed further if we assume independence in nodal positions, i.e., $\Pr[r_1 \leqslant x_1,\cdots,r_N \leqslant x_N] = \prod_{n=1}^{N}\Pr[r_n \leqslant x_n]$, with corresponding pdf

$$g_{\{r_1,\cdots,r_N\}}(x_1,\cdots,x_N) = \prod_{n=1}^{N} g_{r_n}(x_n).$$

Then, the expected number of links in Eq. (9) reduces to

$$E[L] = \int_V \prod_{n=1}^{N} dr_n g_{r_n}(r_n) \sum_{i=1}^{N}\sum_{j=i+1}^{N} f(|r_i - r_j|) = \sum_{i=1}^{N}\sum_{j=i+1}^{N}\int_V dr_i \int_V dr_j g_{r_i}(r_i)g_{r_j}(r_j)\, f(|r_i - r_j|).$$

Assuming identical distributions $\Pr[r_n \leqslant x] = \Pr[r \leqslant x]$ and a same pdf $g_{r_n}(x) = g_r(x)$ for any node $n \in \mathcal{N}$, the corresponding link density $p$ is

$$p = \frac{E[L]}{L_{\max}} = \int_V dq \int_V ds\, g_r(q) g_r(s)\, f(|q-s|). \tag{10}$$

When the nodes are placed uniformly at random inside a $D$-dimensional rectangular hyperprism with edge lengths $Z_1, Z_2, \cdots, Z_D$ and volume $v = \prod_{d=1}^{D} Z_d$, so that $g_r(x) = \frac{1}{v}$, the integral in Eq. (10) can be analytically evaluated. Numerical evaluation of the more general expression given in Eq. (10) is rather straightforward, given that the i.i.d. nodal location density $g_r(x)$ is known. Choosing the uniform density $g_r(x) = \frac{1}{v}$ and a square of size $Z$ in 2D, the link density $p$ for an arbitrary distance function $f(r)$ is derived in Ref. [12]. Appendix A generalizes the link density $p$ to $D$ dimensions in a rectangular hyperprism. Because in Cartesian coordinates the distance between nodes $r_i$ and $r_j$ is given by $|r_i - r_j|^2 = \sum_{d=1}^{D} (r_{i_d} - r_{j_d})^2$, we denote $f(|r_i - r_j|) = h(|r_i - r_j|^2)$ to simplify the notation and Eq. (10) becomes

$$p = 2^D \int_0^{Z_1} du_1 \cdots \int_0^{Z_D} du_D \prod_{d=1}^{D} \frac{(Z_d - u_d)}{Z_d^2} h\left(\sum_{d=1}^{D} u_d^2\right), \tag{11}$$

where $u_d$ is the location variable in dimension $d$. The analytical derivation of Eq. (11) with $D = 2$ for general distance function $f(r) = h(r^2)$ is presented in Appendix A. Analytical derivation of Eq. (11) in higher dimensions $D > 2$ is cumbersome.

Instead of integrating over the positions $u_d$ in $D$ dimensions, we can integrate over the distance between two nodes and Eq. (11) is rewritten as the expectation of the distance function $f(R)$

$$p = E[f(R)] = \int_0^{r_{\max}} f(r) g_R(r) dr, \tag{12}$$

where the random variable $R \in [0, r_{\max}]$ of the distance has pdf $g_R(r)$. Even though Eqs. (11) and (12) are the same when nodes are independently placed at random inside a hyperprism, Eq. (12) is implicit and assumes the knowledge of the pdf $g_R(r)$.

### B. Link density approximation in a hypercube

A number of papers, e.g., Refs. [14,15,19], study the boundary effects of the considered space on the nodal degree and connectivity. In this work, the boundary effects are captured in the derivation of the link density $p$ in Eq. (11). We approximate here the link density $p$ in Eq. (11) for the case of a hypercube with $Z_1 = \cdots = Z_D = Z$ to study the effects of the nodes located at the corners of the hyperprism. Assuming that one vertex of the hypercube is at the origin, we consider a part of a hypersphere of radius $Z$ and center at the origin, which is entirely enclosed by the hypercube. Thus, in the 2D space, the link density $p_{\text{square-2D}}$ in a square is approximated by the link density $p_{\text{circle/4}}$ in a quarter of a circle while in 3D, the link density $p_{\text{cube-3D}}$ in a cube is approximated by the link density $p_{\text{sphere/8}}$ in an octant of a sphere. In Appendix B 1 and B 2

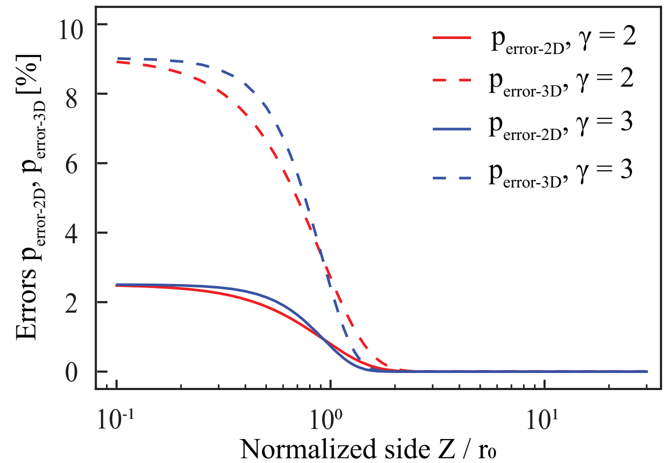


FIG. 3. Error from approximate solution of link density in a square and a cube for $r_c = 1$ m, $K = 4.65 \times 10^{-5}$, and $\beta = -103.3$ dB.

we derive the link densities $p_{\text{circle/4}}$ and $p_{\text{sphere/8}}$, respectively, leading to

$$p_{\text{square-2D}} = \int_0^1 h(Zx)(2\pi x - 8x^2 + 2x^3)dx + p_{\text{error-2D}}, \tag{13}$$

$$p_{\text{cube-3D}} = \int_0^1 h(Zx)(4\pi x^2 - 6\pi x^3 + 8x^4 - x^5)dx + p_{\text{error-3D}}, \tag{14}$$

where $p_{\text{error-2D}}$ and $p_{\text{error-3D}}$ denote the errors introduced by the approximations in the 2D and 3D spaces, respectively.

Appendix B 3 solves $p_{\text{circle/4}}$ and $p_{\text{sphere/8}}$ for any value of $\gamma$ of the distance function (7). Comparing the link densities $p_{\text{circle/4}}$ and $p_{\text{sphere/8}}$ with the exact link densities $p_{\text{square-2D}}$ and $p_{\text{cube-3D}}$ derived from Eq. (11), the errors $p_{\text{error-2D}}$ and $p_{\text{error-3D}}$ are determined and shown in Fig. 3.

Figure 3 illustrates that the approximation of the link density $p_{\text{square-2D}}$ in the 2D space, as shown in Eq. (13), is more accurate than the link density $p_{\text{cube-3D}}$ in the 3D space, as shown in Eq. (14), regardless of $\gamma$. Indeed, the partial circle/sphere does not cover the whole area/volume of the square/cube and thus the nodes located in the distant corner are neglected. In general, the volume ratio of the inscribed hypersphere over the hypercube is equal to $v_D = \frac{\pi^{\frac{D}{2}}}{\Gamma(\frac{D}{2}+1)2^D}$, which is independent of the size $Z$ and rapidly tends to zero with $D$. For example, $v_2 = \frac{\pi}{4} = 0.7854$, $v_3 = \frac{\pi}{6} = 0.5236$, $v_4 = \frac{\pi^2}{32} = 0.3084$, $v_5 = \frac{\pi^2}{60} = 0.1644$, and $v_6 = \frac{\pi^3}{384} = 0.0807$. In other words, the higher the number of dimensions $D$, the worse the approximation and the larger the ratio $1 - v_D$ of the neglected "corner" volume. This explains why the error $p_{\text{error-3D}}$ is larger than the error $p_{\text{error-2D}}$.

Additionally, Fig. 3 depicts that even though the fraction of the uncovered area/volume is fixed for any $Z$, the approximations are accurate when $\frac{Z}{r_0}$ is greater than about 2 and 2.8, for $\gamma = 3$ and $\gamma = 2$, respectively. In particular, the approximations are accurate when the link densities $p_{\text{square-2D}}$ and $p_{\text{cube-3D}}$ are greater than about 0.8 and 0.5, respectively, and regardless of $\gamma$. Apparently, the corner nodes that are neglected from the approximate link densities $p_{\text{circle/4}}$ and $p_{\text{sphere/8}}$, have negligible influence on the link densities $p_{\text{square-2D}}$ and $p_{\text{cube-3D}}$, respectively, for large $Z$. Typically, links involving a corner node are characterized by a large distance $r$ and, consequently, a small connection probability that tends to zero for large $R$. Furthermore, beside the size $Z$ of the hypercube, the accuracy also depends on $\gamma$: since the distance function $f(r)$ decreases in $\gamma$ (for $r > r_0$) the impact of the corner nodes on the link density is less prominent for large $\gamma$.

When the nodes are placed independently and uniformly at random in a square of size $Z$, the pdf of the distance between two nodes $g_R(r)$ in Eq. (12) is equal to Ref. [21], for $0 < r \leqslant Z$,

$$g_R(r) = \frac{2\pi Z^2 r - 8Zr^2 + 2r^3}{Z^4}, \tag{15}$$

and for $Z < r \leqslant \sqrt{2}Z$,

$$g_R(r) = \frac{-2r^3 + 8Zr\sqrt{r^2 - Z^2}}{Z^4} + \frac{2Z^2 r\left(4\arcsin\left(\frac{Z}{r}\right) - 2 - \pi\right)}{Z^4}. \tag{16}$$

After the transformation $r = Zx$, the $p_{\text{circle/4}}$ and $p_{\text{error-2D}}$ terms in Eq. (13) are again found, using Eqs. (15) and (16) in Eq. (12), respectively. Therefore, the approximation (13) indeed neglects all links between nodes located at the corner of the square. Similar conclusions apply for any number of dimensions $D$.

## IV. EVALUATION WITH SIMULATIONS

For the distance function $f(r)$ in Eq. (8), the link density $p$ in Eq. (11) is simulated and the influence of the path loss exponent $\gamma$ and of the geometry of the prism in 2D and 3D is studied. We also show that the link density $p$ is *accurately approximated* by a Fréchet distribution. We denote the side ratio $\omega = \frac{Z_2}{Z_1}$ and the height ratio $\delta = \frac{Z_3}{Z_1}$ and assume that $Z_1 \geqslant Z_2$ and $Z_1 \geqslant Z_3$, implying that $0 < \omega \leqslant 1$ and $0 < \delta \leqslant 1$.

### A. Impact of environment

Figure 4 shows the link density $p_{2D}$ and $p_{3D}$ in the 2D and 3D spaces versus the normalized length $\frac{Z_1}{r_0}$ of side $Z_1$ w.r.t. the maximum allowed distance $r_0$, when varying $\gamma$. Figure 4 shows that the link density $p$ increases with the loss exponent $\gamma$ when $\frac{Z_1}{r_0}$ is less than a threshold, that depends on the dimension and prism's shape and size. For $Z_1 < r_0$, the majority of distances between two nodes obeys $r < r_0$ and thus the link density $p$ behaves similarly to the distance function $f(r)$ for $r < r_0$ ($\frac{1}{e} \leqslant f(r) \leqslant 1$). When $Z_1$ is sufficiently larger than $r_0$, the distance between two nodes $r$ can be much greater than $r_0$ and thus the distance function $f(r)$ can take any value between zero and one. This is also the reason why after a $\frac{Z_1}{r_0}$ threshold value, the link density $p$ behaves the same for any $\gamma$.

When $Z_1 \sim r_0$, border effects play a role, as previously explained. Equation (3) demonstrates that $r_0$ decreases with $\gamma$ and the border effects influence the link density when $\gamma$ decreases, for a particular value of $Z_1$. However, when $Z_1$ is sufficiently larger than $r_0$, the borders have no impact

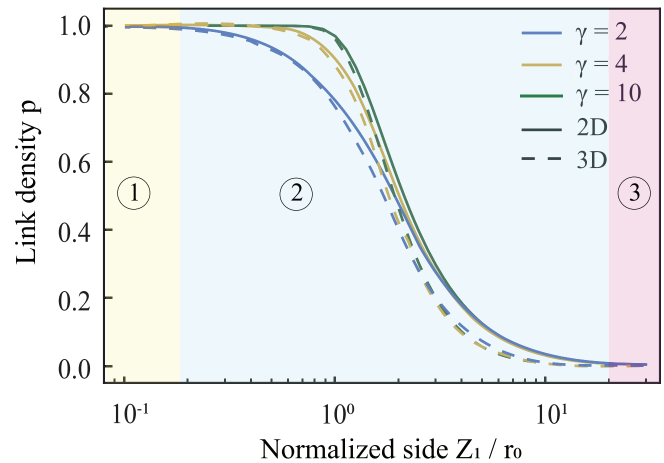


FIG. 4. Impact of the path loss exponent $\gamma$ on the link density $p$ in the 2D and 3D spaces for $\omega = 0.75$, $\delta = 0.5$, $r_c = 1$ m, $K = 4.65 \times 10^{-5}$, and $\beta = -103.3$ dB.

on the link density. Moreover, $\lim_{\gamma\to\infty} f(r) = 1_{r<r_0}$ and for $\gamma \to \infty$ in Eq. (3), it holds that $r_0 = r_c$. Thus, the limit of $\gamma \to \infty$ in Eq. (11), results in $p = 0$, due to the restriction $r > r_c$ in wireless networks. Additionally, for $\frac{Z_1}{r_0} \to 0$ the link density $p \to 1$ because either the distance $r$ between any two nodes is very small ($r \to 0$), as an effect of $Z_1 \to 0$, and thus $\lim_{r\to 0} f(r) = 1$, or because $\lim_{r_0\to\infty} f(r) = 1$, as a result of $r_0 \gg Z_1$.

The link density in Fig. 4 versus $x = \frac{Z_1}{r_0}$ is fitted by

$$p(x) = 1 - e^{-\left(\frac{x-a}{b}\right)^{-c}}, \tag{17}$$

where $F_X(z) = \Pr[X \leqslant z] = e^{-\left(\frac{z-a}{b}\right)^{-c}} 1_{z\geqslant a}$ is a scaled Fréchet distribution of r.v. $X \geqslant 0$ and the parameters $a \in (-\infty, \infty)$, $b \in (0, \infty)$, and $c \in (0, \infty)$ are the location of the minimum, scale and shape of the Fréchet distribution, respectively. The values of $(a_{2D}, b_{2D}, c_{2D})$ and $(a_{3D}, b_{3D}, c_{3D})$ fitting the link density $p$ curves in the 2D and 3D spaces, respectively, as shown in Fig. 4, are given in Table I along with their standard error. The root-mean-square error (RMSE) of each fit is less than 0.01 and emphasizes the remarkably high accuracy of the Fréchet approximation (17). The dependence of the fitting parameters $a, b, c$ on $\gamma$, $\omega$, and $\delta$, shown in Appendix C, highlights that the parameter $c \approx D$ approximately equals the dimensions $D$, when the border effects are minimal.

In summary, the Fréchet distribution in Eq. (17) very accurately approximates the link density with a distance function

TABLE I. Fit values for Eq. (17) with $\omega = 0.75$, $\delta = 0.5$, $r_c = 1$ *m*, $K = 4.65 \times 10^{-5}$, and $\beta = -103.3$ dB.

| $\gamma$ | 2 | 4 | 10 |
|---|---|---|---|
| $a_{2D}$ | $-1.09 \pm 0.02$ | $-0.40 \pm 0.02$ | $0.00 \pm 0.03$ |
| $b_{2D}$ | $2.54 \pm 0.02$ | $2.05 \pm 0.02$ | $1.79 \pm 0.03$ |
| $c_{2D}$ | $2.28 \pm 0.01$ | $2.18 \pm 0.02$ | $1.99 \pm 0.03$ |
| $a_{3D}$ | $-2.00 \pm 0.02$ | $-1.27 \pm 0.03$ | $-0.29 \pm 0.01$ |
| $b_{3D}$ | $3.31 \pm 0.03$ | $2.80 \pm 0.03$ | $1.94 \pm 0.01$ |
| $c_{3D}$ | $3.50 \pm 0.02$ | $3.62 \pm 0.03$ | $2.82 \pm 0.01$ |

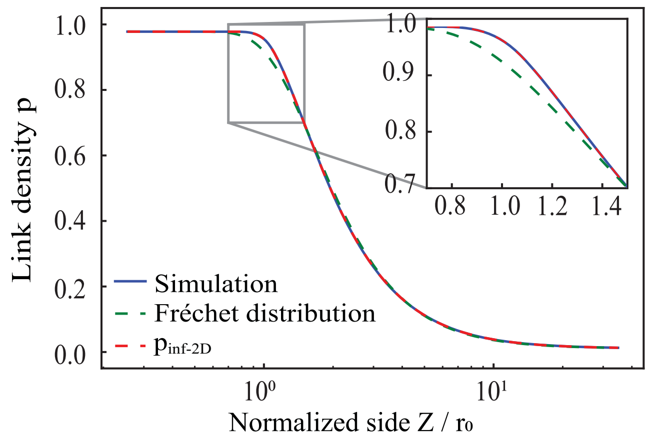


FIG. 5. Link density comparison between the simulation of Eq. (11) (blue), the fitting of a Fréchet (green) and the polynomial solution from Eqs. (18) and (19) for a square of size $Z$ and $\gamma \to \infty$.

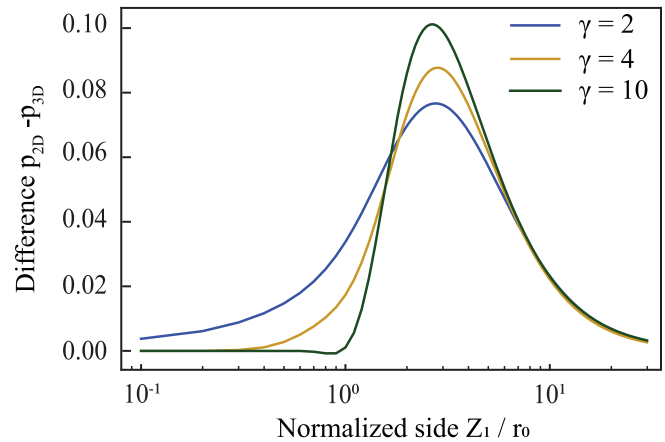


FIG. 6. Difference $p_{2D} - p_{3D}$ of link density between the 2D and 3D spaces, for different values of $\gamma$ when $\omega = 0.75$, $\delta = 0.5$, $r_c = 1$ m, $K = 4.65 \times 10^{-5}$, and $\beta = -103.3$ dB.

$f(r) = e^{-(\frac{r}{r_0})^\gamma}$ for any physically interesting $\gamma$ and all prism geometries. Therefore, this new insight motivates the use of Eq. (17), instead of Eq. (11), in applications.

### B. Hard RGG in a square and the Fréchet distribution

To motivate the accurate fitting with the Fréchet distribution, we consider the special case of a hard RGG with $\lim_{\gamma\to\infty} f(r) = 1_{r<r_0}$. Then, the link density in Eq. (12) for a square of size $Z$ is equal to $p_{\text{inf-2D}} = G_R(r) = \Pr[R \leqslant r_0]$. Setting $x = \frac{Z}{r_0}$, Eq. (12) leads to, for $0 < r_0 \leqslant Z$,

$$p_{\text{inf-2D}}(x) = \frac{x^{-4}}{2} - \frac{8x^{-3}}{3} + \pi x^{-2}, \tag{18}$$

for $Z < r_0 \leqslant \sqrt{2}Z$,

$$p_{\text{inf-2D}}(x) = -\frac{x^{-4}}{2} + \frac{8(x^{-2}-1)^{3/2}}{3} + 4\sqrt{x^{-2}-1} + 4x^{-2}\arcsin x - (2+\pi)x^{-2} + \frac{1}{3}, \tag{19}$$

and for $r_0 > \sqrt{2}Z$, the link density $p_{\text{inf-2D}} = 1$.

The link density $p_{\text{inf-2D}}$ can be approximated by a Poisson point process (PPP), where $N$ nodes are uniformly distributed in a circle with radius $Z$. The probability in a PPP to have an isolated node equals $p_{\text{iso}} = e^{-\rho\pi r_0^2}$, where $\rho = \frac{N}{\pi Z^2}$ is the node density. Hence, the probability to have a link is

$$\Pr[R \leqslant r_0] = 1 - e^{-\rho\pi r_0^2}.$$

Because $p_{\text{inf-2D}} = \Pr[R \leqslant r_0]$ we can write using $x = \frac{Z}{r_0}$:

$$p_{\text{inf-2D-PPP}}(x) = 1 - e^{-(\frac{x}{b})^{-2}}, \tag{20}$$

where $b = \sqrt{N}$. Thus, $p_{\text{inf-2D-PPP}}(x)$ satisfies Eq. (17) with parameters (0, $\sqrt{N}$, 2) of the Fréchet distribution.

Figure 5 shows the link density for a square and for $\gamma \to \infty$ as derived (i) via simulations from Eq. (11), (ii) by fitting Eq. (11) with the Fréchet distribution in Eq. (20), and (iii) by Eqs. (18) and (19). Figure 5 illustrates that the Fréchet distribution approximates the link density in Eq. (11) *remarkably well*. Specifically, the fit of the Fréchet distribution with parameters (0, 1.65, 2) yields an RMSE of 0.005 and the difference on a plot is hardly visible. The Fréchet distribution is only slightly inaccurate when $r_0 \sim Z$, which is due to border effects that are not captured in Eq. (20). Additionally, Fig. 5 shows that the link density in Eqs. (18) and (19) are the exact solutions of Eq. (11). The simplicity of the Fréchet distribution compared to the complexity of the exact link density (11) is remarkable and motivates its use in applications.

### C. Difference in dimensions

Figure 4 illustrates that the link density $p_{3D} \leqslant p_{2D}$, regardless of the value of $\gamma$. We identify three regions for $\frac{Z_1}{r_0}$, indicated by the encircled numbers in Fig. 4:

(1) $p_{2D} = p_{3D} = 1$: the distance between any two nodes is small enough to provide a link.

(2) $p_{2D}$ upper bounds $p_{3D}$: the 3D distance between any two nodes is always larger than or equal to its projection in the 2D space.

(3) $p_{2D} \to 0$ and $p_{3D} \to 0$: the distance between any two nodes is too large to provide a link.

Figure 6 shows the link density difference $p_{2D} - p_{3D}$ of the Fréchet approximation (17). The difference $p_{2D} - p_{3D}$ behaves similarly for any $\gamma$ and it is maximized at around $\frac{Z_1}{r_0} = 2.75$, which is dependent on the geometry given by $\omega$ and $\delta$.

### D. Impact of shape and volume

The maximum distance between two nodes is

$$r_{2D,\max} = \sqrt{Z_1^2 + Z_2^2} = Z_1\sqrt{1+\omega^2},$$

$$r_{3D,\max} = \sqrt{Z_1^2 + Z_2^2 + Z_3^2} = Z_1\sqrt{1+\omega^2+\delta^2}. \tag{21}$$

For a given value of the side $Z_1$ and the side length $Z_2$ (and thus $\omega$), an increase of the height $Z_3$ (and thus $\delta$), reduces the link density $p_{3D}$ because the maximum distance $r_{3D,\max}$ between two nodes increases, as also shown in Eq. (21). Figure 7 illustrates the difference $p_{2D} - p_{3D}$ in link density between the 2D and 3D spaces, which increases with $\delta$. For $\delta \ll \omega$, e.g., $\omega = 1$ and $\delta = 0.1$, the effect of $Z_3$ (and thus

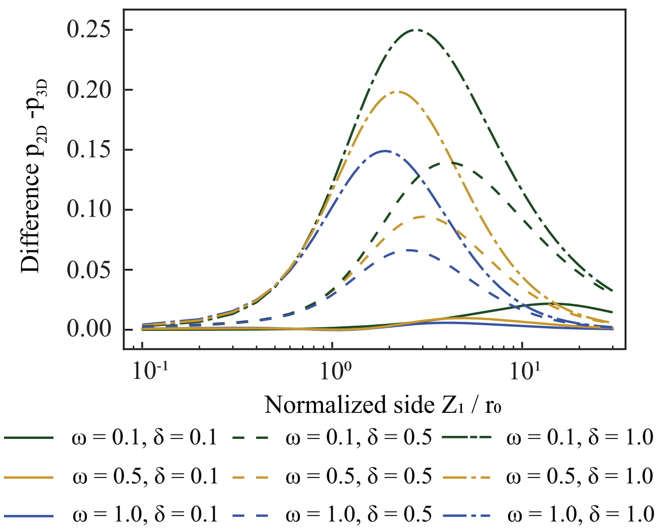


FIG. 7. Difference $p_{2D} - p_{3D}$ of link density between the 2D and 3D spaces for different combinations of $\omega$ and $\delta$ when $\gamma = 2$, $r_c = 1$ m, $K = 4.65 \times 10^{-5}$, and $\beta = -103.3$ dB.

$\delta$) in Eq. (21) becomes negligible and hence $p_{2D} - p_{3D} \approx 0$. Additionally, an increase of $\delta$ shifts the maximum difference $p_{2D} - p_{3D}$ to a smaller $\frac{Z_1}{r_0}$ value because the shape of the prism becomes more symmetrical.

Similarly, based on Eq. (21), when considering a constant side $Z_1$ and height $Z_3$ (and thus $\delta$), an increase of the side length $Z_2$ (and thus $\omega$) increases the size of the rectangle and prism in the horizontal plane, given by $Z_1$ and $Z_2$. Thus, the maximum distances $r_{2D,\max}$ and $r_{3D,\max}$ between two nodes increase and hence both the link densities $p_{2D}$ and $p_{3D}$ decrease. Figure 7 depicts that the difference $p_{2D} - p_{3D}$ also decreases with an increase of $\omega$, which implies that $p_{2D}$ reduces faster than $p_{3D}$.

## V. APPLICATION TO DRONE NETWORKS

In future telecommunication networks, drones are expected to provide coverage in a disaster area or when a ground base station fails or to serve incidental traffic hot spots. When a swarm of drones is deployed, the drones in the swarm are expected to communicate with each other to avoid collisions and exchange necessary information for collaborative tasks. Thus, any drone should be able to reach any other drone in the swarm to establish a connected network. While many studies in literature focus on deploying a swarm of drones to provide coverage and/or capacity to the access network, the connectivity among the drones is usually ignored [22,23]. In this section, the minimum number $N_{\min}$ of drones that need to be deployed for a connected network is computed, based on the link density $p$. We model the drone network with a RGG. Because drones can be deployed at the same altitude or at different altitudes, e.g., for scenarios where both terrestrial users and users in high-rise buildings are considered, the 2D and the 3D spaces are considered.

Previously we have shown that the link density $p$ depends on $\gamma$, $\omega = \frac{Z_2}{Z_1}$, $\delta = \frac{Z_3}{Z_1}$ as well as on $r_0$ and thus on $\beta$. To evaluate the impact of each parameter, we refer to a baseline scenario $S_0$, which can describe a realistic drone network and we propose a set of scenarios by unilaterally varying the parameters of the baseline scenario to an extreme value, as shown in Table II. We simulate $10^4$ realizations for each scenario and for each prism's size $Z_1$ and derive the link density $p$ and the minimum number of nodes $N_{\min}$, such that the network is connected. We measure connectivity via the giant component size, which equals the number of nodes in the largest cluster of the network divided by the total number of nodes $N$ in the network. When the giant component size is equal to 1, the network is connected. The number of nodes in the largest cluster are found after first creating $N$ clusters, where the $n$th cluster contains the $n$th node. Then, we merge the clusters that have at least one common node. We repeat the cluster mergers until no cluster shares a common node with another cluster. The largest cluster is the one that contains the most nodes. We regard the network as connected when the giant component size is greater than or equal to 0.99.

TABLE II. Scenario configurations.

| Scenario | $\gamma$ | $\beta$ | $\omega$ | $\delta$ |
|---|---|---|---|---|
| $S_0$ | 2 | −127 dB | 0.75 | 0.5 |
| $S_\gamma$ | 4 | −127 dB | 0.75 | 0.5 |
| $S_\beta$ | 2 | −80 dB | 0.75 | 0.5 |
| $S_\omega$ | 2 | −127 dB | 0.1 | 0.5 |
| $S_\delta$ | 2 | −127 dB | 0.75 | 0.1 |

Table II shows the chosen parameters for the considered scenarios. Scenario $S_0$ describes a network with a good propagation environment (e.g., in high altitude), with a typical minimum required channel gain $\beta$ and drones placed in a space where the horizontal plane is larger than the vertical plane. In Scenario $S_\gamma$, the propagation environment is worse (i.e., the path loss exponent $\gamma$ is higher) than the one in Scenario $S_0$, which can indicate that the drones are flying closer to the ground where there are many obstacles. The effects of a higher minimum required channel gain $\beta$ compared to Scenario $S_0$ are captured in Scenario $S_\beta$, implying an increase of the noise power and/or a reduction of the SNR threshold and/or a reduction of the transmission power. Scenarios $S_\omega$ and $S_\delta$ capture the impact of the space where the drones are located. Specifically, in Scenario $S_\omega$, the horizontal plane is narrower than the vertical plane while in Scenario $S_\delta$, the vertical plane is much narrower than the horizontal plane.

Figure 8 shows the link density $p$ and the minimum number of nodes $N_{\min}$ as derived from simulating the above-mentioned scenarios. The fitted curves in Fig. 8 are deduced from all scenarios and follow a power law $N_{\min} = ap^b$ where $(a_{2D}, b_{2D})$ and $(a_{3D}, b_{3D})$ are the fitting parameters with their standard error, in the 2D and 3D spaces, respectively:

$$\begin{aligned} a_{2D} &= 5.14 \pm 0.32, \; b_{2D} = -1.12 \pm 0.04, \\ a_{3D} &= 4.35 \pm 0.27, \; b_{3D} = -1.23 \pm 0.04. \end{aligned} \tag{22}$$

The RMSE of the fitting is 2.96 and 2.73 for the 2D and 3D spaces, respectively.

Figure 8 shows that the minimum number of nodes $N_{\min}$ needed for connectivity does not depend on the dimension $D$ of the space (2D or 3D), but only on the value of the

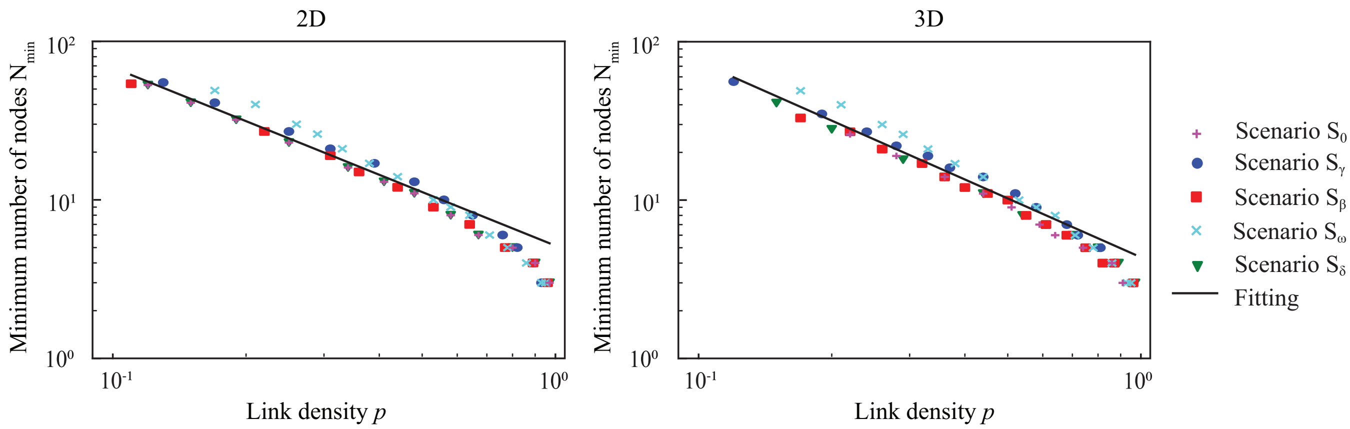


FIG. 8. Minimum number of nodes $N_{\min}$ needed for connectivity in respect to the link density $p$, for the scenarios shown in Table II, as well as the fitting curves given by Eq. (22).

link density $p$. However, Fig. 8 also shows that the minimum number of nodes $N_{\min}$ needed for connectivity can vary per scenario when the link density is less than about 0.5. For example, when comparing Scenarios $S_0$ and $S_\omega$, we observe that a reduction of the parameter $\omega$ from 0.75 to 0.1, increases the minimum number of nodes $N_{\min}$ by about 10, when the link density is equal to 0.2. Also, for link density $p > 0.7$, the fitted curves are overestimating the minimum number of nodes $N_{\min}$. Therefore, we can conclude that Eq. (22) provides a rough approximation of the minimum number of nodes $N_{\min}$.

## VI. CONCLUSIONS

We have computed the link density in $D$-dimensional RGGs, generated by a general distance function $f(r)$ and we have demonstrated its remarkably accurate approximation by the Fréchet distribution function (17) for any path loss exponent $\gamma$ and any prism geometry. Also, we indicated that the link density $p_{2D}$ in the 2D space upper bounds that in the 3D space, when the same propagation environment and size of the horizontal plane are considered. Finally, based on the giant component size, we have found that the minimum number of nodes $N_{\min}$ needed for connectivity is a power law of the link density $p$. The above-mentioned insights can be helpful in applications requiring the deployment of a swarm of drones. For example, when the size of and the propagation conditions in a disaster or crowded area that require coverage or extra capacity are known, $N_{\min}$ provides an estimation on the minimum number of drones that should be deployed to have a connected swarm of drones.

While the Fréchet distribution (17) accurately approximates the link density $p$, a method to easily derive the fitting values for different scenarios is left for further research. Here, we assumed that the fixed nodes are independent and uniformly distributed in the $D$-dimensional space. In future work, we will investigate how the node mobility and the spatial distribution influence the minimum number of nodes $N_{\min}$ needed for connectivity. In most wireless networks, the links are dependent due to interference. Thus, the impact of interference and potential ways to mitigate interference will also be addressed.

## ACKNOWLEDGMENTS

This work is part of NExTWORKx, a collaboration between TU Delft and KPN on future telecommunication networks.

## APPENDIX A: LINK DENSITY IN A RECTANGULAR HYPERPRISM

When nodes are placed uniformly at random inside the prism, the link density $p$, given by

$$p = \frac{E[L]}{L_{\max}} = \int_V dq \int_V ds\, g_r(q) g_r(s)\, f(|q-s|),$$

can be written as

$$p = \int_V \frac{dq}{v} \int_V \frac{ds}{v} f(|q-s|), \tag{A1}$$

where $q = (x_1, x_2, \dots, x_D)$ and $s = (y_1, y_2, \dots, y_D)$ are the coordinates of two random nodes and $f(|q-s|)$ is the probability that two nodes at distance $|q-s|$ are connected by a link. In Cartesian coordinates, the distance $|x-y|^2 = \sum_{d=1}^{D}(x_d - y_d)^2$. To simplify the notation, we denote $h(|x-y|^2) = f(|x-y|)$ and the integral in Eq. (A1) becomes

$$p = \int_0^{Z_1} dx_1 \int_0^{Z_1} dy_1 \cdots \int_0^{Z_D} dx_D \int_0^{Z_D} dy_D \frac{h\left[\sum_{d=1}^{D}(x_d - y_d)^2\right]}{\prod_{d=1}^{D} Z_d^2}. \tag{A2}$$

We use symmetry to reduce the $2D$-fold integral to a $D$-fold integral. We concentrate on the integration over the $d$ dimension and denote $w_d^2 = \sum_{k=1;k\neq d}^{D}(x_k - y_k)^2$ that is independent of dimension $d$ (i.e., of $x_d$ and $y_d$),

$$\int_0^{Z_d} dx_d \int_0^{Z_d} dy_d\; h\left[(x_d - y_d)^2 + \sum_{\substack{k=1\\k\neq d}}^{D}(x_k - y_k)^2\right]$$
$$= \int_0^{Z_d} dx_d \int_0^{Z_d} dy_d\; h\left[(x_d - y_d)^2 + w_d^2\right].$$

After substitution $u_d = x_d - y_d$, where $y_d$ is kept constant, followed by partial integration, we obtain

$$\int_0^{Z_d} dx_d \int_0^{Z_d} dy_d\, h\left[(x_d - y_d)^2 + \sum_{\substack{k=1\\k\neq d}}^{D}(x_k - y_k)^2\right]$$
$$= 2\int_0^{Z_d} du_d\, (Z_d - u_d) h\left[u_d^2 + \sum_{\substack{k=1\\k\neq d}}^{D}(x_k - y_k)^2\right].$$

Any other dimension can be treated similarly and the integral in Eq. (A2) is reduced to the integral

$$p = 2^D \int_0^{Z_1} du_1 \cdots \int_0^{Z_D} du_D \prod_{d=1}^{D} \frac{(Z_d - u_d)}{Z_d^2} h\left(\sum_{d=1}^{D} u_d^2\right). \tag{A3}$$

We can calculate the link density (A3) numerically for any dimension $D$ and analytically for $D = 2$,

$$p_{\text{rect-2D}} = \frac{4}{(Z_1Z_2)^2} \int_0^{Z_1} du_1 \int_0^{Z_2} du_2\, (Z_1 - u_1) \times (Z_2 - u_2)\, h\big(u_1^2 + u_2^2\big). \tag{A4}$$

Transformed to polar coordinates $p_{\text{rect-2D}} = \frac{4(p_A+p_B+p_C)}{(Z_1Z_2)^2}$, where

$$p_A = \int_0^{Z_2} h(r) r dr \int_0^{\frac{\pi}{2}} (Z_1 - r\cos\theta)(Z_2 - r\sin\theta) d\theta,$$
$$p_B = \int_{Z_2}^{Z_1} h(r) r dr \int_0^{\arcsin\left(\frac{Z_2}{r}\right)} (Z_1 - r\cos\theta) \times (Z_2 - r\sin\theta) d\theta,$$
$$p_C = \int_{Z_1}^{\sqrt{Z_1^2+Z_2^2}} h(r) r dr \int_{\arccos\left(\frac{Z_1}{r}\right)}^{\arcsin\left(\frac{Z_2}{r}\right)} (Z_1 - r\cos\theta) \times (Z_2 - r\sin\theta) d\theta.$$

Solving the $\theta$-integrals of $p_A$, $p_B$, and $p_C$ separately, with

$$Q(\theta) = \int (Z_1 - r\cos\theta)(Z_2 - r\sin\theta) d\theta$$
$$= Z_1Z_2\theta + Z_1 r\cos\theta - Z_2 r\sin\theta - \frac{r^2}{4}\cos(2\theta) + c,$$

where $c$ is an integration constant, leads to the link density in a rectangle

$$p_{\text{rect-2D}} = \frac{4}{Z_1^2 Z_2^2}(p_A + p_B + p_C), \tag{A5}$$

with

$$p_A = \int_0^{Z_2} h(r) r \left[\frac{Z_1Z_2\pi}{2} - (Z_1 + Z_2) r + \frac{r^2}{2}\right] dr,$$
$$p_B = \int_{Z_2}^{Z_1} h(r) r \left[\frac{Z_1Z_2\pi - Z_2^2}{2} - Z_1 r - Z_1Z_2 \arccos\left(\frac{Z_2}{r}\right) + Z_1\sqrt{r^2 - Z_2^2}\right] dr,$$
$$p_C = \int_{Z_1}^{\sqrt{Z_1^2+Z_2^2}} h(r) r \left[\frac{Z_1Z_2\pi - Z_1^2 - Z_2^2}{2} - Z_1Z_2 \arccos\left(\frac{Z_1}{r}\right) - Z_1Z_2 \arccos\left(\frac{Z_2}{r}\right) + Z_1\sqrt{r^2 - Z_2^2} + Z_2\sqrt{r^2 - Z_1^2} - \frac{r^2}{2}\right] dr.$$

## APPENDIX B: LINK DENSITY APPROXIMATION IN A HYPERCUBE

For $Z_1 = Z_2 = \cdots = Z_D = Z$, Eq. (11) becomes

$$p_{\text{Dcube}} = \frac{2^D}{Z^{2D}} \int_0^{Z} du_1 \cdots \int_0^{Z} du_D \prod_{d=1}^{D} (Z - u_d) h\left(\sum_{d=1}^{D} u_d^2\right).$$

We transform the integral from Cartesian to polar coordinates using the transformation in [24]. Because the boundaries of the hypercube are a bit more involved, we consider the integral over a part of the hypersphere of radius $Z$ and center at the origin, that is entirely enclosed by the hypercube,

$$p_{\text{Dcircle}} = \frac{2^D}{Z^{2D}} \int_0^{R} h(r) r^{D-1} dr \int_0^{\frac{\pi}{2}} d\varphi_1 \cdots \int_0^{\frac{\pi}{2}} d\varphi_{D-1} \times \prod_{d=1}^{D-1}\left(Z - r\cos\varphi_d \prod_{j=1}^{d-1}\sin\varphi_j\right) \times \left(Z - r\sin\varphi_{D-1}\prod_{j=1}^{D-2}\sin\varphi_j\right) \times \prod_{d=1}^{D-1}\sin^{D-1-d}\varphi_d \tag{B1}$$

and provides a lower bound for $p_{\text{Dcube}}$ of the hypercube.

### 1. Two dimensions

Setting $D = 2$ and using $\varphi_1 = \theta$ in Eq. (B1), assuming that the coordinates of the circle with radius $Z$ are given in $(r, \theta)$, we find for the 2D space

$$p_{\text{circle/4}} = \frac{4}{Z^4} \int_0^{Z} h(r) r dr \int_0^{\frac{\pi}{2}} (Z - r\cos\theta) \times (Z - r\sin\theta) d\theta. \tag{B2}$$

Using Eq. (A5) and the transformation $r = Zx$, Eq. (B2) becomes

$$p_{\text{circle/4}} = \int_0^1 h(Zx)(2\pi x - 8x^2 + 2x^3) dx. \tag{B3}$$

### 2. Three dimensions

In the 3D space, we use $\varphi_1 = \theta$ and $\varphi_2 = \phi$, assuming that the coordinates of the sphere with radius $Z$ are given in

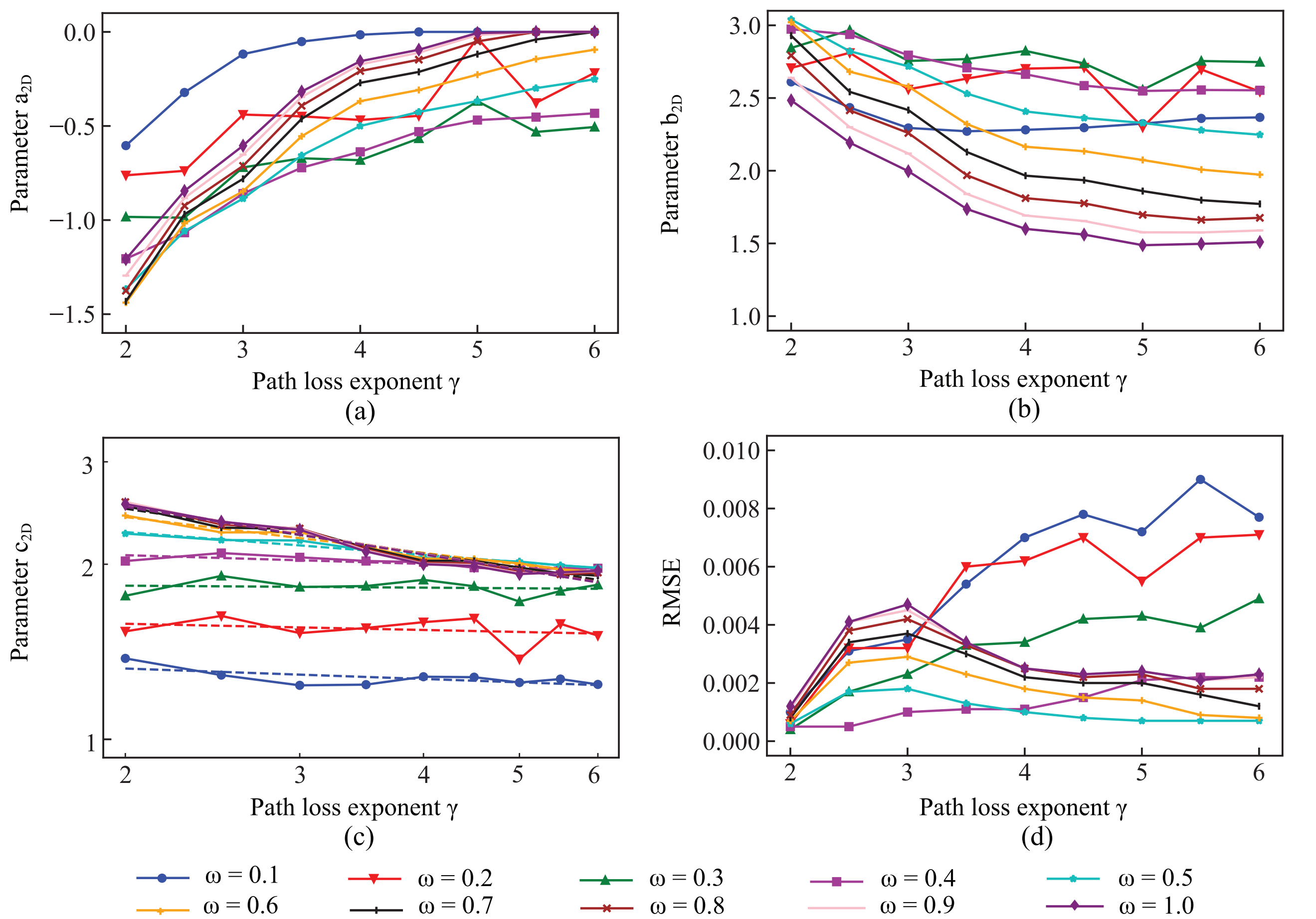


FIG. 9. Panels (a), (b), and (c) illustrate the fitting parameters $a_{2D}$, $b_{2D}$, and $c_{2D}$, respectively, for different values of $\omega$ and $\gamma$, while panel (d) illustrates the RMSE of each fit. Panel (c) is in log-log scale.

$(r, \theta, \phi)$. Using Eq. (B1) we find

$$p_{\text{sphere}/8} = \frac{8}{Z^6}\int_0^Z h(r)r^2dr \int_0^{\frac{\pi}{2}} \sin\theta(Z - r\cos\theta)d\theta \times \int_0^{\frac{\pi}{2}} (Z - r\cos\phi\sin\theta)(Z - r\sin\phi\sin\theta)d\phi. \tag{B4}$$

The $\phi$-integral becomes

$$\int_0^{\frac{\pi}{2}} (Z - r\sin\theta\cos\phi)(Z - r\sin\theta\sin\phi)d\phi = \frac{\pi}{2}Z^2 - 2rZ\sin\theta + \frac{r^2\sin^2\theta}{2}. \tag{B5}$$

Substituting Eq. (B5) in Eq. (B4), we get

$$p_{\text{sphere}/8} = \frac{8}{Z^6}\int_0^Z h(r)r^2dr \int_0^{\frac{\pi}{2}} \sin\theta(Z - r\cos\theta) \times \left(\frac{\pi}{2}Z^2 - 2rZ\sin\theta + \frac{r^2\sin^2\theta}{2}\right)d\theta.$$

After substitution of the $\theta$ integral

$$\int_0^{\frac{\pi}{2}} \sin\theta(Z - r\cos\theta)\left(\frac{\pi}{2}Z^2 - 2rZ\sin\theta + \frac{r^2\sin^2\theta}{2}\right)d\theta = \frac{\pi Z^3}{2} - \frac{3\pi Z^2 r}{4} + Zr^2 - \frac{r^3}{8}$$

and letting $r = Zx$, we arrive at

$$p_{\text{sphere}/8} = \int_0^1 h(Zx)(4\pi x^2 - 6\pi x^3 + 8x^4 - x^5)dx. \tag{B6}$$

### 3. Formal solution of $p_{\text{Dcircle}}$ in Eq. (B1) in higher dimensions

Both integrals (B3) and (B6) are of the form

$$p_{\text{Dcircle}} = \int_0^1 h(Zx)p_n(x)dx,$$

where $p_n(x) = \sum_{j=0}^n a_j x^j$ is a polynomial of degree $n$ in $x$. The integral can be elegantly solved if $h(z)$ is an entire function.[2] Here, we confine to $h(z) = e^{-\beta z^\gamma}$, which is not an entire function if $\gamma$ is not an integer. With $\alpha = \beta R^\gamma$, the general

[2]An entire (also called integral) function is a complex function without singularities in the finite complex plane (see Ref. [25, Chapter VIII]).

TABLE III. Fit values for parameter $c_{3D}$.

| $\omega$ | $\psi$ | $\xi$ | RMSE |
|---|---|---|---|
| 0.1 | $1.38 \pm 0.05$ | $0.06 \pm 0.03$ | 0.03 |
| 0.2 | $1.62 \pm 0.11$ | $0.04 \pm 0.05$ | 0.07 |
| 0.3 | $1.85 \pm 0.08$ | $0.01 \pm 0.03$ | 0.05 |
| 0.4 | $2.15 \pm 0.04$ | $0.05 \pm 0.01$ | 0.03 |
| 0.5 | $2.48 \pm 0.03$ | $0.13 \pm 0.01$ | 0.02 |
| 0.6 | $2.79 \pm 0.05$ | $0.21 \pm 0.01$ | 0.03 |
| 0.7 | $2.98 \pm 0.07$ | $0.26 \pm 0.02$ | 0.03 |
| 0.8 | $3.05 \pm 0.09$ | $0.27 \pm 0.02$ | 0.04 |
| 0.9 | $3.06 \pm 0.10$ | $0.28 \pm 0.03$ | 0.05 |
| 1.0 | $3.03 \pm 0.10$ | $0.27 \pm 0.03$ | 0.05 |

integral above becomes[3]

$$p_{D\text{circle}} = \sum_{j=0}^{n} a_j \int_0^1 e^{-\alpha r^\gamma} r^j dr. \tag{B7}$$

From the definitions in Refs. [26, 6.5.3,6.5.4], $\Gamma(a,z) = \Gamma(a)[1 - z^a\gamma^*(a,z)]$ and Refs. [26, 6.5.29], it follows that

$$\gamma^*(a,z) = \frac{1}{\Gamma(a)} \sum_{k=0}^{\infty} \frac{(-z)^k}{k!(a+k)}. \tag{B8}$$

A second powerful series is

$$\gamma^*(a,z) = e^{-z} \sum_{k=0}^{\infty} \frac{z^k}{\Gamma(a+1+k)}. \tag{B9}$$

The entire incomplete $\Gamma$ function $\gamma^*(a,z)$ is an entire function so that Eqs. (B8) and (B9) converge for all $a$ and all $z$. With this preparation, we return to the integral (B7) and find, after Taylor expansion of the exponential and invoking Eq. (B8),

$$p_{D\text{circle}} = \sum_{j=0}^{n} a_j \sum_{k=0}^{\infty} \frac{(-\alpha)^k}{k!(j+1+\gamma k)}$$
$$= \frac{1}{\gamma} \sum_{j=0}^{n} a_j \gamma^*\left(\frac{j+1}{\gamma}, \alpha\right) \Gamma\left(\frac{j+1}{\gamma}\right).$$

The other series (B9) leads to

$$p_{D\text{circle}} = \frac{e^{-\alpha}}{\gamma} \sum_{j=0}^{n} a_j \sum_{k=0}^{\infty} \frac{\Gamma\left(\frac{j+1}{\gamma}\right)}{\Gamma\left(\frac{j+1}{\gamma}+1+k\right)} \alpha^k.$$

Using $\frac{\Gamma(x+m)}{\Gamma(x)} = \prod_{l=0}^{m-1}(x+l)$ then results into a factorial series (see, e.g., Ref. [27]),

$$p_{D\text{circle}} = e^{-\alpha} \sum_{j=0}^{n} \frac{a_j}{j+1} \sum_{k=0}^{\infty} \frac{\alpha^k}{\prod_{l=1}^{k}\left(\frac{j+1}{\gamma}+l\right)},$$

that converges for all $\alpha$.

[3] We can transform the integral by letting $x = \alpha r^\gamma$ and $r = (\frac{x}{\alpha})^{\frac{1}{\gamma}} = \alpha^{-\frac{1}{\gamma}} x^{\frac{1}{\gamma}}$, thus $dr = \alpha^{-\frac{1}{\gamma}} \frac{1}{\gamma} x^{\frac{1}{\gamma}-1} dx$ and

$$\int_0^1 e^{-\alpha r^\gamma} r^j dr = \frac{\alpha^{-\frac{j+1}{\gamma}}}{\gamma} \int_0^\alpha e^{-x} x^{\frac{j+1}{\gamma}-1} dx.$$

The right-hand side integral can be written in terms of the incomplete $\Gamma$ integral is $\Gamma(a,z) = \int_z^\infty e^{-x} x^{a-1} dx$, which is *not* an entire function.

## APPENDIX C: FRÉCHET FITTING OF THE LINK DENSITY

The highly accurate Fréchet distribution for the link density,

$$p(x) = 1 - e^{-\left(\frac{x-a}{b}\right)^{-c}},$$

has parameters $a, b, c$, that depend upon the path loss exponent $\gamma$ and the prism geometry.

For the 2D space, Fig. 9 shows the influence of the path loss exponent $\gamma$ on the fitting parameters $(a_{2D}, b_{2D}, c_{2D})$ for different values of $\omega = \frac{Z_2}{Z_1}$. In particular, Fig. 9 shows that $-1.5 < a_{2D} \leqslant 0$, $1 < b_{2D} < 3$ and $1 < c_{2D} < 3$. Also, for a given $\omega$ and $\gamma$ it holds $|\frac{a_{2D}}{b_{2D}}| < 0.5$. Additionally, the plot of $c_{2D}$ versus the path loss exponent $\gamma$ in Fig. 9(c) roughly illustrates two regimes for $\omega \leqslant 0.3$ and for $\omega > 0.3$. The lower values of $\omega \leqslant 0.3$ indicate the convergence of the 2D space toward the 1D space in which the link density $p$ is more confined by the border effects. Hence, the Fréchet fitting is slightly less accurate for $\omega \leqslant 0.3$ than

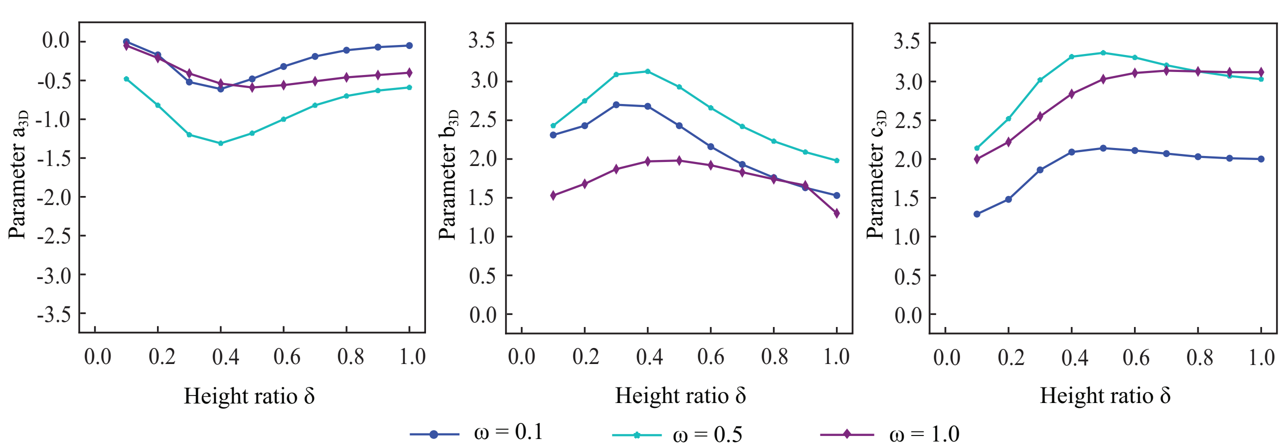


FIG. 10. Fitting parameters $(a_{3D}, b_{3D}, c_{3D})$ for different values of $\omega$ and $\delta$ and for $\gamma = 5$.

for higher values of $\omega > 0.3$ and reflected by the RMSE in Fig. 9(d), although the maximum RMSE <0.01 is still very low.

The parameter $c_{2D}$ represents the shape of the Fréchet distribution and Fig. 9(c) exhibits that the parameter $c_{2D}$ follows closely a power law $c_{2D}(\gamma) = \psi\gamma^{-\xi}$. The values and the standard error of the fitting parameters $(\psi, \xi)$ and the RMSE of each fitting are given in Table III. Additionally, Fig. 9(c) illustrates that for $\omega > 0.3$, the parameter $c_{2D} \geqslant 2$ and approaches $c_{2D} \to 2$ for higher values of $\gamma$, because of the minimal border effects as explained in Sec. III B. Generally, when the border effects are minimal, the parameter $c_{2D}$ is approximately equal to the dimensions $D = 2$.

A similar analysis for the 3D space in Fig. 10 illustrates the dependence of $(a_{3D}, b_{3D}, c_{3D})$ on $\delta = \frac{Z_3}{Z_1}$ for $\gamma = 5$. Similarly to the 2D space, the parameter $c_{3D}$ is approximately equal to the dimensions $D = 3$ for graphs where the border effects are minimal, i.e., for large $\omega$, $\delta$ and $\gamma$. Additionally, when $\omega \to 0$ and for large $\delta$ (to minimize the border effects) the 3D space reduces to the 2D space and thus $c_{3D} \approx c_{2D} \approx 2$. Due to symmetry, when $\delta \to 0$ and for large $\omega$, it again holds $c_{3D} \approx c_{2D} \approx 2$.


[1] B. Bollobas, *Random Graphs*, 2nd ed. (Cambridge University Press, Cambridge, UK, 2011)

[2] E. N. Gilbert, Random plane networks, J. Soc. Ind. Appl. Math. **9**, 533 (1961).

[3] M. Wilsher, C. P. Dettmann, and A. Ganesh, Connectivity in one-dimensional soft random geometric graphs, Phys. Rev. E **102**, 062312 (2020).

[4] M. Haenggi, J. G. Andrews, F. Baccelli, O. Dousse, and M. Franceschetti, Stochastic geometry and random graphs for the analysis and design of wireless networks, IEEE J. Sel. Areas Commun. **27**, 1029 (2009).

[5] C. Bettstetter, On the minimum node degree and connectivity of a wireless multihop network, in *Proceedings of the 3rd ACM International Symposium on Mobile Ad Hoc Networking and Computing, MobiHoc '02, Lausanne, Switzerland* (ACM, New York, NY, 2002), pp. 80–91.

[6] M. Barthelemy, Spatial networks, Phys. Rep. **499**, 1 (2011).

[7] G. A. Pagani and M. Aiello, From the grid to the smart grid, topologically, Physica A **449**, 160 (2016).

[8] V. Erba, S. Ariosto, M. Gherardi, and P. Rotondo, Random geometric graphs in high dimension, Phys. Rev. E **102**, 012306 (2020).

[9] J. Hoebeke, I. Moerman, B. Dhoedt, and P. Demeester, An overview of mobile ad hoc networks: Applications and challenges, Commun. Network **3**, 60 (2004).

[10] I. Bekmezci, O. K. Sahingoz, and S. Temel, Flying ad-hoc networks (FANETs): A survey, Ad Hoc Netw. **11**, 1254 (2013).

[11] J. Dall and M. Christensen, Random geometric graphs, Phys. Rev. E **66**, 016121 (2002).

[12] P. Van Mieghem, Paths in the simple random graph and the Waxman graph, Probab. Eng. Inf. Sci. **15**, 535 (2001).

[13] P. Fan, G. Li, K. Cai, and K. B. Letaief, On the geometrical characteristics of wireless ad-hoc networks and its application in network performance analysis, IEEE Trans. Wireless Commun. **6**, 1256 (2007).

[14] B. Bakhshi and S. Khorsandi, Node connectivity analysis in multi-hop wireless networks, in *Proceedings of the IEEE Wireless Communications and Networking Conference, Sydney, NSW* (IEEE, Piscataway, NJ, 2010), pp. 1–6.

[15] Z. Khalid, S. Durrani, and J. Guo, A tractable framework for exact probability of node isolation and minimum node degree distribution in finite multihop networks, IEEE Trans. Veh. Technol. **63**, 2836 (2014).

[16] R. Hekmat and P. Van Mieghem, Connectivity in wireless ad-hoc networks with a log-normal radio model, Mobile Networks Appl. **11**, 351 (2006).

[17] S. C. Ng, G. Mao, and B. D. O. Anderson, Critical density for connectivity in 2D and 3D wireless multihop networks, IEEE Trans. Wireless Commun. **12**, 1512 (2013).

[18] Z. Khalid and S. Durrani, Connectivity of three dimensional wireless sensor networks using geometrical probability, in *Proceedings of the Australian Communications Theory Workshop (AusCTW)* (IEEE, Piscataway, NJ, 2013), pp. 47–51.

[19] C. P. Dettmann and O. Georgiou, Random geometric graphs with general connection functions, Phys. Rev. E **93**, 032313 (2016).

[20] A. Goldsmith, *Wireless Communications* (Cambridge University Press, Cambridge, UK, 2005).

[21] S. Lellouche and M. Souris, Distribution of distances between elements in a compact set, Stats **3**, 1 (2020).

[22] M. Mozaffari, W. Saad, M. Bennis, and M. Debbah, Efficient deployment of multiple unmanned aerial vehicles for optimal wireless coverage, IEEE Commun. Lett. **20**, 1647 (2016).

[23] A. V. Savkin and H. Huang, Asymptotically optimal deployment of drones for surveillance and monitoring, Sensors **19**, 2068 (2019).

[24] L. E. Blumenson, A derivation of $n$-dimensional spherical coordinates, Am. Math. Mon. **67**, 63 (1960).

[25] E. C. Titchmarsh, *The Theory of Functions* (Oxford University Press, Amen House, London, 1964).

[26] M. Abramowitz and I. A. Stegun, *Handbook of Mathematical Functions* (Dover Publications, New York, 1968).

[27] P. Van Mieghem, Binet factorial series and extensions to Laplace transforms, Delft University of Technology, Technical report no. 20210202 (http://arxiv.org/abs/2102.04891) (2021).